Available online at www.sciencedirect.com
ScienceDirect
Composites Science and Technology 67 (2007) 438–452
COMPOSITES SCIENCE AND TECHNOLOGY
www.elsevier.com/locate/compscitech

Effects of nonlinear viscoelastic behaviour and loading rate on transverse cracking in CFRP laminates

The Hoang Nguyen [a,b], Denys Gamby [a,*]

[a] Laboratoire de Mécanique et de Physique des Matériaux, ENSMA, 1 Av Clément Ader, BP 40109, 86961 Futuroscope, Chasseneuil Cedex, France
[b] Department of Aeronautical Engineering, HoChiMinh City University of Technology, 268 Ly Thuong Kiet Street, District 10, HoChiMinh City, Viet Nam

Received 6 December 2005; received in revised form 23 August 2006; accepted 27 August 2006
Available online 24 October 2006

Abstract

The progressive multiplication of matrix transverse cracks in cross-ply laminates made of long carbon fibre reinforced polymer (CFRP) is addressed in this study. Monotonic tensile tests performed on $[0_3/90_3]_S$ laminates at 120 °C have shown a marked dependence of cracking development on loading rate. This paper aims to assess the impact of the material nonlinearity on the loading rate sensitivity of the damaging process. A ''shear-lag'' damage analysis, using the nonlinear correspondence principle and appropriate failure criteria, is carried out to numerically predict the cracking evolution. This work shows that, though important, the material nonlinearity of the undamaged material does not significantly enhance the loading rate sensitivity of the cracking process and it cannot explain alone the phenomenon. On the other hand, taking into account the loading rate dependence of the critical strength, together with the R-curve effect, which gives good predicted cracking curves, suggests that the observed rate effect pertains to the viscoelastic character of the damaged material in the process zone close to crack fronts.

Keywords: A. Polymer–matrix composites; B. Non-linear behaviour; C. Transverse cracking; C. Failure criterion; Loading rate effect

1. Introduction

High-performance CFRP composite laminates are used in several aircraft structural parts due to weight saving and high lifetime demands in aeronautic applications. The next generation of supersonic aircraft, for instance Concorde's successor, will travel at speeds that cause significant heating of the aircraft structure owing to friction in the atmosphere. During a flight at a speed of Mach 2, the maximum surface temperature will range between 100 °C and 130 °C, depending on the considered part of the structure. Under such service conditions involving high temperature and mechanical loads, the candidate composites may display a variety of damage modes, such as matrix cracking, fibre breakage, interfacial debonding between matrix and fibre, or delamination between plies. In cross-ply laminates subjected to tensile thermo-mechanical loadings, transverse matrix cracking is usually the first damage mechanism to be observed and it creates initiation sites for further and potentially more harmful damage events. Therefore, transverse matrix cracking must be assessed and monitored in order to guarantee the structural integrity.

The recent literature contains few experimental and analytical studies of the influence of viscoelastic behaviour and loading rate on matrix cracking. Time dependent matrix cracking in transverse plies of cross-ply carbon/epoxy laminates was experimentally investigated and modelled in [1–5]. Under quasi static loading, it is observed that the matrix cracking growth rate depends upon the loading rate at temperatures of 110 °C [1] and 120 °C [4] or even at room temperature [2,3]. A probabilistic failure model involving loading rate has been proposed by Ogi and Takao [1], giving a good agreement between experimental results and

* Corresponding author. Tel.: +33 05 49 49 82 39; fax: +33 05 49 49 82 38.
E-mail addresses: hoangnuli@vnn.vn (T.H. Nguyen), gamby@lmpm.ensma.fr (D. Gamby).

0266-3538/$ - see front matter © 2006 Elsevier Ltd. All rights reserved.
doi:10.1016/j.compscitech.2006.08.027

numerical simulations under monotonic loading. However, it provides little physical understanding, though the cracking behaviour can be phenomenologically described.

The evolution of transverse matrix cracking in a carbon/epoxy composite laminate of the type $[0_m/90_n]_S$ will be addressed in this research. A significant influence of loading rate on the damaging process at 120 °C has been previously experimentally brought out [4]. Several phenomena might explain this effect, notably the viscoelastic behaviour of the undamaged material in the 90°-plies and that of the damaged material around crack tip vicinities. Some numerical simulations meant to display the effect of possible factors have been proposed in previous papers: a one-dimensional (1D) linear viscoelastic shear-lag approach, which takes into account thermal stresses, has been implemented in [6,7]. Several failure criteria (critical stress, critical strain and Reiner-Weissenberg or critical free energy density), used to describe cracking evolution as a function of load level assuming a constant loading rate, give very close numerical results. The failure criteria can properly display the loading rate effect only if a stress rate dependence is incorporated into the critical values. Then a two-dimensional linear viscoelastic analysis has been developed in [6]. The numerically predicted crack density curves show that, even if the 2D stress state is taken into account, the viscoelastic character of the undamaged material is not marked enough to explain alone the influence of the loading rate on cracking curves. The improvement brought about by the incorporation of thermal stresses is not significant at the considered temperature for the studied material.

However, creep-recovery tests conducted at the studied temperature reveal that the material at hand displays a marked nonlinear viscoelastic behaviour. This raises some further questions, such as: how do transverse cracks grow if the nonlinear viscoelastic character of material is taken into account? And can the material nonlinearity increase the influence of loading rate on cracking?

This paper aims to provide preliminary answers to these questions. First, the experimental results concerning the crack density as a function of applied tensile load, assuming a constant stress rate, are described in Section 2. Then, by using a simplified 1D Schapery model, a material characterization procedure is proposed in Section 3 in order to approximately identify the nonlinear stress–strain relationship of the material in the 90°-plies. A damage growth analysis is carried out in Section 4. Some simplifying assumptions are proposed in order to apply the nonlinear correspondence principle. A numerical program strategy meant to predict the cracking evolution is detailed in Section 4.4. Some discussions and conclusions are contained in the last section.

According to the knowledge of the authors, in the recent literature, very few works present a viscoelastic model involving the nonlinear behaviour of the undamaged material to describe the transverse cracking on the ply scale. Zhang et al. [8] have proposed a micromechanical model involving the nonlinear viscoelastic behaviour of the matrix. The "localized" matrix cracking on the fibre scale is well modelled by a so-called "smeared crack" approach. However, this model using a repeating independent unit cell containing only one "elastic" fibre does not deal with the non-homogeneous damage kinetics induced by the ply-scale transverse cracks.

2. Experimental results [4]

A carbon/epoxy composite laminate made of IM7/977-2 system with $[0_3/90_3]_S$ stacking sequence and a nominal ply thickness of 0.125 mm, has been studied. The coupons, 140 mm long and 20 mm wide, were designed and provided by CCR-EADS (Corporate Research Centre, France, of the European Aeronautic Defence and Space Company). The material is made up of long carbon fibres possessing a high modulus of elasticity and of a two-phase toughened epoxy resin. The thermo-elastic properties of the unidirectional ply experimentally obtained at 120 °C are given in Table 1.

Monotonic uniaxial tensile tests were conducted on the cross-ply laminates at a temperature of 120 °C to measure transverse matrix crack density as a function of applied load. Three different loading rates (1.3216 MPa/min, 132.16 MPa/min and 1321.6 MPa/min), producing cross-head velocities of 0.01 mm/min ($\sim 10^{-7}$ s^{-1}), 1 mm/min ($\sim 10^{-5}$ s^{-1}) and 10 mm/min ($\sim 10^{-4}$ s^{-1}), respectively, were prescribed.

The tests were stopped several times before the failure of specimens to count the number of transverse cracks (N) on the useful length (L_u) of the polished edges by using an optical microscope; the average crack density, defined by $\rho = N/L_u$, can thus be obtained.

Here the useful length is the " gage length", i.e. the length along which transverse cracks are counted under an optical microscope (see Fig. 1 for details). While the total length of the specimen is 140 mm, the 80 mm-value is chosen as the "useful length" in this study. The specimen

Table 1
Elastic properties and coefficients of thermal expansion (CTE) of the unidirectional ply at 120 °C

Property		Value
Longitudinal modulus (GPa)	E_{11}	148
Transverse modulus (GPa)	E_{22}	7.12
In-plane Poisson's ratio	ν_{12}	0.326
In-plane shear modulus (GPa)	G_{12}	3.3
Longitudinal CTE (10^{-6} °C)	α_1	0.23
Transverse CTE (10^{-6} °C)	α_2	30

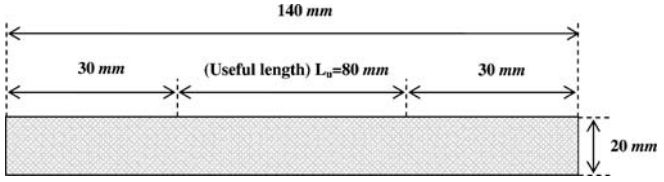

Fig. 1. Specimen geometry.

is clamped in the testing machine at its ends along 30 mm-length end-tabs.

The experimental results are presented in Fig. 2. At this temperature, loading rate has a significant influence on cracking. First, it can be seen that the occurrence of the first cracks is delayed when the loading rate increases. Namely, the higher the stress rate, the higher the first ply failure stress. It is also observed that the higher the loading rate the greater the tensile strength. Moreover, the crack density increases more rapidly as a function of applied stress level if the loading rate decreases. This crack density involves "long cracks" only. A "long crack" is defined as a "transverse crack" which spans the entire thickness of the central 90°-layer of the laminate. Therefore, at a same applied stress level, a "long crack" or a "transverse crack" is distinguished from a "short crack" by its length in comparison with the 90°-layer thickness. In fact, transverse cracks emanate from short cracks: these first propagate in the thickness direction, then in the width direction. However the first kind of propagation is very rapid (nearly instantaneous), and cannot be observed. When the 90° layer is thick enough, the propagation along the width direction is also very rapid. However, for thin 90° layers (one elementary ply), the widthwise propagation is slow, which means that most transverse cracks do not span the entire specimen width. The widthwise length of each individual transverse crack can be measured by stopping the test at regular times, removing the specimen, then taking its X-ray picture. This was not systematically done in this work, but a quantitative study of individual crack lengths was performed in the same laboratory by Lafarie-Frenot et al. [24], for instance.

Here, the only observed phenomenon was the transverse crack multiplication along the specimen length. It was quantified by the number of such cracks appearing on the specimen edge.

The two cracking phases, "crack initiation" and "crack propagation", are experimentally distinguished by the manner in which the transverse cracks appear. During the initiation phase (or cracking onset), it can be observed (by an optical microscope) that some early transverse cracks, randomly distributed along the specimen length, appear in the central 90°-layer. This phase possesses a stochastic nature due to the inhomogeneities of the material (such as local fiber fraction, local flaw concentration in the matrix, etc.). After this initiation phase, when the applied load increases, the number of transverse cracks increases and the crack distribution becomes more regular. The crack propagation phase (or cracking development) corresponds to this stage.

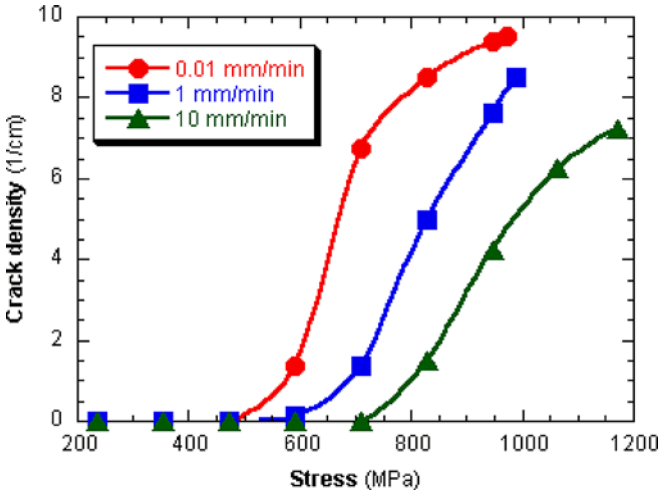

Fig. 2. Effect of loading rate on matrix cracking evolution during monotonic tensile tests at 120 °C [4].

In Fig. 2, the averaged crack density is plotted against the applied tensile stress at 120 °C for three loading rates. Each test corresponding to one loading rate was repeated twice in order to estimate the measurement scatter. The measurements obtained for both specimens were found to be very similar: the scatter on crack numbers might be evaluated between 10 per cent for lower load values and 1 per cent at the end of the tests. More details are given in [7]. It can be noted that the slope of the first two curves corresponding to 0.01 and 1 mm/min ($\dot{\varepsilon} = 3 \times 10^{-7}\ s^{-1}$ and $3 \times 10^{-5}\ s^{-1}$ respectively) are not very different, whereas the third curve (10 mm/min or $\dot{\varepsilon} = 3 \times 10^{-4}\ s^{-1}$) has a markedly lower slope. It should be remarked that the three investigated strain rates are in the lower part of the range of the possible values which can be sustained by this material (up to $\dot{\varepsilon} = 1500\ s^{-1}$), [25].

3. Material characterization

3.1. Constitutive equations

The Schapery model is selected to describe the nonlinear viscoelastic response of the unidirectional 90°-plies. The three-dimensional constitutive equations of the Schapery model can be expressed as [9]:

$$\varepsilon_i(t) = g_{ij}^{(0)}\left(\sigma_{eq}(t)\right) J_{0ij}\sigma_j(t) + g_{ij}^{(1)}\left(\sigma_{eq}(t)\right) \times \int_{0^-}^{t} \Delta J_{ij}\left(\psi_{ij}(t) - \psi_{ij}(\tau)\right) \frac{d}{d\tau}\left[g_{ij}^{(2)}\left(\sigma_{eq}(\tau)\right)\sigma_j(\tau)\right] d\tau \quad (1)$$

$i = (1, 2, \ldots, 6)$ and $j = (1, 2, \ldots, 6)$, where the single-index stresses and strains are defined by:

$$\sigma_1 = \sigma_{11},\quad \sigma_2 = \sigma_{22},\quad \sigma_3 = \sigma_{33},\quad \sigma_4 = \sigma_{23},\quad \sigma_5 = \sigma_{13},\quad \sigma_6 = \sigma_{12}$$

$$\varepsilon_1 = \varepsilon_{11},\quad \varepsilon_2 = \varepsilon_{22},\quad \varepsilon_3 = \varepsilon_{33},\quad \varepsilon_4 = 2\varepsilon_{23},\quad \varepsilon_5 = 2\varepsilon_{13},\quad \varepsilon_6 = 2\varepsilon_{12}$$

The reduced times are given by:

$$\psi_{ij}(t) = \int_0^t \frac{du}{a_{ij}\left(\sigma_{eq}(u)\right)};$$

$J_{ij}(t) = J_{0ij} + \Delta J_{ij}(t)$ are the creep functions of the material; $g_{ij}^{(0)}$, $g_{ij}^{(1)}$, $g_{ij}^{(2)}$ and a_{ij} are the nonlinearizing functions which depend on the so-called "equivalent stress" denoted σ_{eq}.

Starting from the set of five stress invariants already employed by Hashin, a suitable definition of the equivalent

stress for transversely isotropic materials is fully discussed by Schapery [10]. For a general three-dimensional stress state, one can choose the equivalent stress in the form of a scalar function accounting for stress interaction:

$$\sigma_{eq} = \left[\sigma_{22}^2 + \sigma_{33}^2 + k_1\sigma_{22}\sigma_{33} + k_2\sigma_{23}^2 + k_3\left(\sigma_{13}^2 + \sigma_{12}^2\right)\right]^{1/2} \quad (2)$$

where k_1, k_2 and k_3 are material constants; for a plane stress state, the equivalent stress can be shown to reduce to $\sigma_{eq} = \left[\sigma_{22}^2 + k_{eq}\sigma_{12}^2\right]^{1/2}$ and possible values for k_{eq} are proposed.

Now, let $f(t) \otimes g(t) = \int_{0^-}^{t} f(t-\tau)\frac{d}{d\tau}g(\tau)\,d\tau$ denote the Stieltjes convolution of time functions $f(t)$ and $g(t)$. If we suppose that the nonlinear behaviour of the material in the 90°-ply group is adequately described by only one stress-dependent function $g_{22}^{(2)}$, which amounts to take $g_{22}^{(0)} = g_{22}^{(1)} = a_{22} = 1$, a one-dimensional functional relationship between stress and strain in the case of a transverse loading can be obtained in the form:

$$\varepsilon(t) = J_{22}(t) \otimes \left[g_2\left(\sigma_{eq}(t)\right)\sigma(t)\right] \quad (3)$$

where $g_2 \equiv g_{22}^{(2)}$; $\sigma \equiv \sigma_2$ and $\varepsilon \equiv \varepsilon_2$ are respectively the applied tensile stress and the strain in the transverse direction; $J_{22}(t)$ is the creep function of the material in the transverse direction such that $E_{22}(t) \otimes J_{22}(t) = H(t)$, $E_{22}(t)$ being the material relaxation function and $H(t)$ being the Heaviside step function. The equivalent stress is given by $\sigma_{eq} = \left[\sigma_{22}^2 + k_{eq}\sigma_{12}^2\right]^{1/2}$, where k_{eq} is a material constant.

3.2. Material characterization procedure

In the linear range, the purely tensile viscoelastic response of the undamaged material in the 90°-layer at 120 °C is described by the creep function $J_{22}(t)$. A generalized Kelvin-Voigt model is chosen to represent this function. The creep function is adequately expressed in the form: $J_{22}(t) = J_{20} + \Delta J_{22}(t)$, where J_{20} is a constant and $\Delta J_{22}(t) = \sum_{n=1}^{N} J_{2n}\left(1 - e^{-t/\tau_n}\right)$ is the transient part in which τ_n is the retardation time related to the amplitude J_{2n}.

The material parameters to be determined are the coefficients involved in the J_{22} function which characterizes the material behaviour in the linear range on one hand, and those involved in the g_2 function which characterizes the material nonlinearity on the other. As J_{22} is taken in the form $J_{22}(t) = J_{20} + \sum_{n=1}^{N} J_{2n}(1 - e^{-t/\tau_n})$, the necessary coefficients are J_{20}, J_{2n}, and τ_n ($n = 1, \ldots, N$). g_2 is defined by the coefficients a_g and b_g. All these coefficients were obtained by comparing the experimental recovery and creep curves with the theoretical predictions given by Eqs. (4) and (5), through a least-square method.

The experimental data from a series of creep-recovery tests conducted on 90°-specimens and provided by A. Vinet (CCR-EADS) were used. An example of identification procedure is detailed in [11]. The tests have been conducted at 120 °C for three stress levels: 10 MPa, 15 MPa and 20 MPa. The strain response curve of the 10 MPa creep-recovery test, performed during a period of a 24-h load

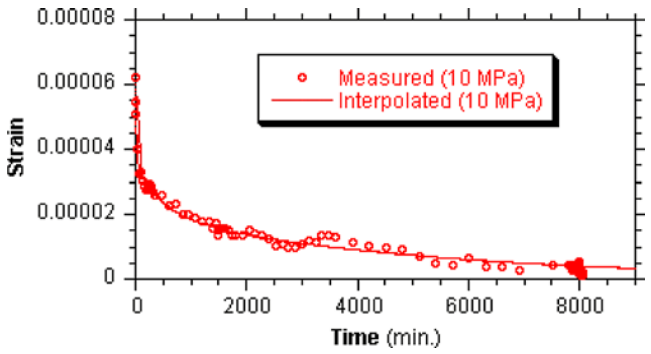

Fig. 3. Comparison between experimental data and interpolation (using $N = 3$) of recovery strain at 120 °C and for 10 MPa applied stress.

followed by a 100-h recovery, is presented in Fig. 3. The time-dependent compliance curves corresponding to the three stress levels reveal that a stress of 10 MPa is probably the bound of the linear viscoelastic regime at 120 °C of such a material, as can be seen in Fig. 4 in which we provide the comparative creep compliance curves for the three stress levels.

For stress levels lower than 10 MPa, all the compliance curves are undistinguishable, whereas the curves for a stress greater than 10 MPa are different from each other.

Therefore, from now on, the experimental data obtained at the stress level of 10 MPa or lower will be treated as linear data, whereas data obtained at higher stress levels will be considered as nonlinear data for the concerned material.

The creep function $J_{22}(t)$ is characterized by using the data in the linear range at 10 MPa.

From Eq. (3), the one-dimensional functional relationship between stress and strain in the case of a transverse loading has the following form:

$$\varepsilon(t) = J_{22}(t) \otimes \left[g_2\left(\sigma_{eq}(t)\right)\sigma(t)\right]$$

where $J_{22}(t) = J_{20} + \Delta J_{22}(t), \sigma_{eq} = \left[\sigma_{22}^2 + k_{eq}\sigma_{12}^2\right]^{1/2}$ with $\sigma_{22} = \sigma$; "$\otimes$" denotes the Stieltjes Convolution. The function g_2 characterizes the nonlinear behaviour of the material. In the linear range where $g_2 = 1$, Eq. (3) becomes:

$$\varepsilon(t) = J_{22}(t) \otimes \sigma(t)$$

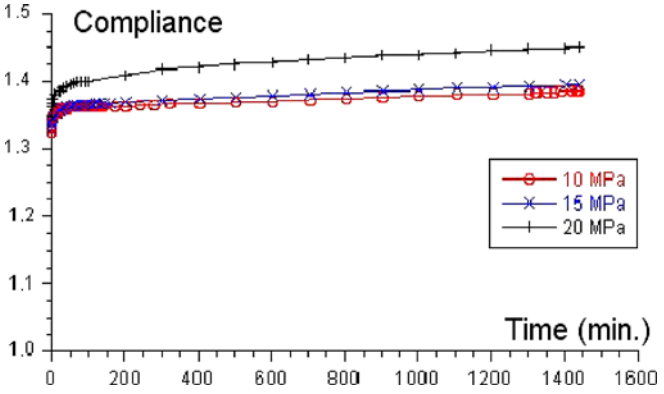

Fig. 4. Compliance (10^{-10} Pa^{-1}) versus time (min) from creep test at several stress levels for IM7/977-2 carbon/epoxy $[90]_n$ laminates, at 120 °C.

The stress history of the creep-recovery tests conducted on the 90°-specimens is:

$$\sigma(t) = \bar{\sigma}_0[H(t) - H(t - t_1)]$$

where t_1 is the creep time. The strain response of the creep-recovery test is then:

$$\begin{aligned}\varepsilon(t) &= J_{22}(t) \otimes \{\sigma; {}^{-}{}_0[H(t) - H(t - t_1)]\} \\ &= \sigma; {}^{-}{}_0\{J_{20}[H(t) - H(t - t_1)] + \Delta J_{22}(t) \otimes [H(t) - H(t - t_1)]\}\end{aligned}$$

The recovery strain is the strain obtained for $t > t_1$. When $t > t_1$ the first term in the bracket in which the parameter J_{20} is involved is zero. This leads to the following relationship between recovery strain and applied stress level:

$$\varepsilon_r(t) = \varepsilon(t > t_1) = \left\{ \underbrace{\Delta J_{22}(t) \otimes H(t)}_{\Delta J_{22}(t)} - \underbrace{\Delta J_{22}(t) \otimes H(t - t_1)}_{\Delta J_{22}(t - t_1)} \right\} \bar{\sigma}_0$$

Therefore, we finally obtain the recovery strain response as:

$$\varepsilon_r(t) = \{\Delta J_{22}(t) - \Delta J_{22}(t - t_1)\}\bar{\sigma}_0 \quad (t > t_1) \tag{4}$$

First, the transient part $\Delta J_{22}(t)$ is obtained from Eq. (4) where $\bar{\sigma}_0 = 10$ MPa is the applied creep-stress and $t_1 = 24$ (h) is the creep time. The experimental recovery strain is fitted to the theoretical curve, Eq. (4), by using the least-square method. Then, the measured creep strain data are used to determine the initial component J_{20} of the creep function from the following relation:

$$J_{20} = \frac{\varepsilon_c(t)}{\bar{\sigma}_0} - \Delta J_{22}(t) \quad (0 < t < t_1)$$

where $\varepsilon_c(t)$ denotes the creep strain response under stress $\bar{\sigma}_0$. The attempt to interpolate the experimental data in the linear range for $\bar{\sigma}_0 = 10$ MPa shows that a good agreement between measured and interpolated points can be obtained by taking three terms ($N = 3$) in the transient part of the creep function. The characterization results are presented in Table 2. The experimental and interpolated curves pertaining to recovery and creep responses are compared in Figs. 3 and 5, respectively.

Next, the experimental recovery curves for other stress levels in the nonlinear range are exploited to characterize the nonlinearizing function g_2. The recovery strain response is now such that:

$$\varepsilon_r(\bar{\sigma}_0, t) = [\Delta J_{22}(t) - \Delta J_{22}(t - t_1)]\bar{\sigma}_0 g_2(\bar{\sigma}_0) \quad (t > t_1) \tag{5}$$

where $g_2 = 1$ in the linear range and $g_2 > 1$ in the nonlinear range. Eq. (5) can be obtained in the same manner as Eq. (4) when $g_2(\bar{\sigma}_0) \neq 1$.

Table 2
Parameters of transverse direction compliance at 120 °C

Term	Coefficient J_{2n} (Pa^{-1})	Retardation time τ_n (min)
0	1.335×10^{-10}	
1	2.500×10^{-12}	20
2	1.555×10^{-12}	500
3	8.034×10^{-12}	5000

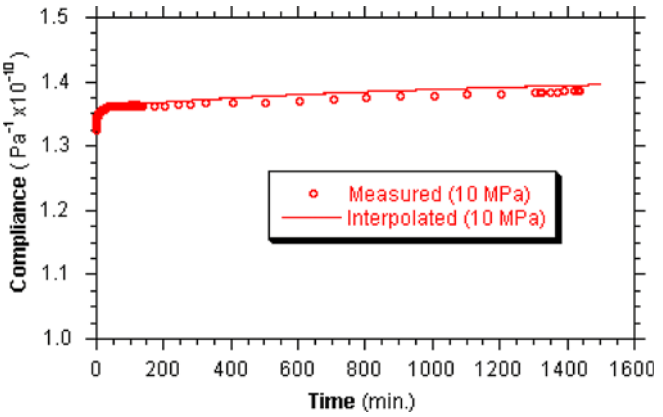

Fig. 5. Comparison between experimental data and interpolation of the creep function at 120 °C and a stress of 10 MPa for the [90°] carbon/epoxy.

The least-square method is applied to the curves ε_r versus time t in order to determine the values of function g_2 at each stress level $\bar{\sigma}_0$ (10 MPa, 15 MPa and 20 MPa). In Fig. 6, the numerical simulations show a good reproduction of the three recovery strain curves corresponding to the three considered stress levels.

The curves in Fig. 6 cannot directly display the nonlinear character of the material; for this purpose, it would be necessary to plot the recovery compliance (recovery strain over applied stress) versus time instead of recovery strain versus time. Here, the same constitutive equation is used for loading and unloading; however, due to the nonlinear behaviour and the time-dependent effects, the stress–strain loading and unloading curves would be different.

All the parameters obtained from the above characterization procedure should finally be assessed by using the creep data (strain or compliance) for all stress levels in the nonlinear range. The creep strain response for any stress level is given in the form: $\varepsilon_c(\bar{\sigma}_0, t) = [J_{20} + g_2(\bar{\sigma}_0)\Delta J_{22}(t)]\bar{\sigma}_0$, where the term in square brackets is the "nonlinear compliance" depending on $\bar{\sigma}_0$. Fig. 7 shows the comparison between interpolated curves and experimental data of the nonlinear compliance for the two considered stress levels $\bar{\sigma}_0 =$

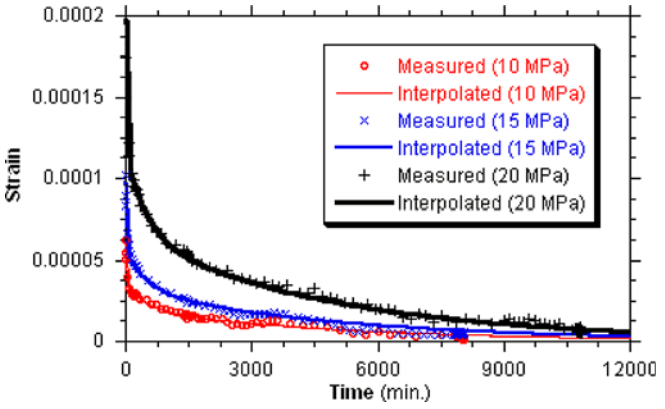

Fig. 6. Comparison between experiment and interpolated strain recovery curves for three constant stress levels in the nonlinear range (10 MPa, 15 MPa and 20 MPa) at 120 °C.

15 MPa and $\bar{\sigma}_0 = 20$ MPa. It can be seen from Fig. 7 that a sufficiently good reproduction of the experimental curves outside the linear range can be obtained by using only one stress-dependent nonlinearizing function g_2.

This function can be represented in the form: $g_2(\sigma) = 1 + a_g\sigma^{b_g}$, where a_g and b_g are material constants characterizing the nonlinear behaviour; and σ should be the equivalent stress in the general case. This interpolation choice was motivated by the trends for g_2 function observed on other similar materials [26]. However, other types of interpolation have been attempted, but they did not lead to significant alteration of the results.

a_g and b_g are mere coefficients involved in the representation of function g_2: in Schapery's model, the Gibbs free energy has a second order expansion related to a nonlinear generalized Maxwell model, and, in the special case used here, $1/g_2$ is the dimensionless nonlinear factor common to all springs of the model [27]. b_g is a dimensionless exponent and a_g is such that the product $a_g\sigma^{b_g}$ has no dimension when σ is in MPa. For instance, when $b_g = 2$, stress σ is in (MPa) and the dimension of a_g is (MPa^{-2}).

The limited number of available values of g_2 for the three considered stress levels (10 MPa, 15 MPa and 20 MPa) are used to fit the above function and result in: $a_g = 1.4 \times 10^{-3}$ and $b_g = 2$ (with stress in MPa). For a stress greater than 20 MPa, the value of g_2 will be extrapolated from the above equation, due to lack of experimental data.

Moreover, in Section 4.3.1, while solving the set of nonlinear ordinary differential equations (31)–(33) with the boundary conditions (34), we found that, if we use an integer exponent (such as 2) rather than a decimal one (such as 2.1, 2.2, etc.), the convergence of the solution is faster. In addition, if we choose a higher order function, for example a fourth power (namely $b_g = 4$), this will lead to a more precise interpolated curve in the stress data range ($0 \leqslant \bar{\sigma}_0 \leqslant 20$ MPa), but this will result in an extrapolated g_2-value increasing too fast outside this stress range ($\bar{\sigma}_0 > 20$ MPa). This increase of g_2 in the range (20 MPa $\leqslant \bar{\sigma}_0 \leqslant$ 40 MPa) seems unrealistic for the class of material at hand. All these reasons explain why a quadratic interpolation was used here.

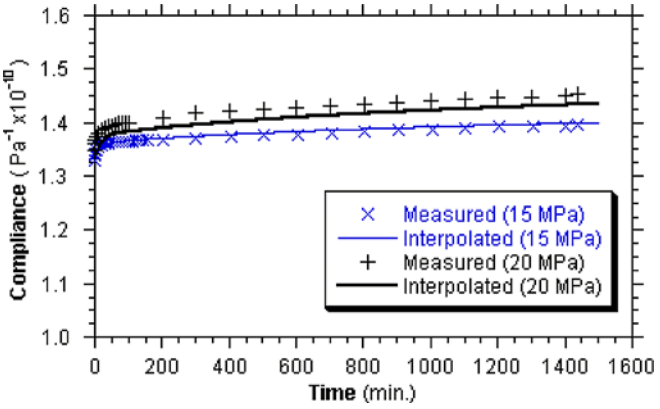

Fig. 7. Comparison between interpolated nonlinear compliance curves and experiment for two stress levels of 15 MPa and 20 MPa at 120 °C.

Fig. 8 presents the variations of g_2 as a function of σ for the material at hand.

4. Crack multiplication analysis

4.1. Preliminary assumptions

Here, we consider $[0_3/90_3]_S$ cross-ply composite laminates, as shown in Fig. 9, possessing one central 90°-layer of thickness $2h_1$ (denoted by superscript (1)) and two outer 0°-layers of thickness h_2 (denoted by superscript (2)). The x, y, z directions are the loading direction, the width direction and the thickness direction, respectively.

The laminate is subjected to an "ideal" progressive repeated loading program (Fig. 10). Each loading "cycle" comprises two phases: a monotonic increase in load of the form $\bar{\sigma}(t) = \dot{\bar{\sigma}} \times t$, $\bar{\sigma}$ being the external applied stress in the x-direction, $\dot{\bar{\sigma}}$ being the constant loading rate, t denoting the time, from zero up to a maximum level, whose amplitude depends on the current cycle, and a phase in which the load decreases to zero; the last is followed by a "recovery" period long enough so that the strains in the layers are allowed to tend to zero before starting a next loading "cycle". The same value of stress rate ($\dot{\bar{\sigma}}$) should be used during the whole loading program.

Some assumptions will be made regarding the damage description. First, under prescribed loading conditions, it is assumed that no delamination occurs and only the transverse cracking phenomenon is considered. Second, the experimental observations show that the matrix crack distribution in the central 90°-layer tends to become periodic when the applied load increases. As a result, the damaged laminate is divided into several unit cells comprised between two existing adjacent cracks, assuming a $2L$ uniform spacing. Due to the symmetry of the cracked laminate, only a half of the unit cell is considered (Fig. 9). In each loading "cycle" (Fig. 10), it is supposed that a new transverse crack appears only when the applied stress reaches its maximum value, and that there is no additional crack formed during the decreasing phase of the applied loading. As a consequence, the "uniform" crack spacing $2L = 2L_k$ is a constant during the time interval $t_k^+ \leqslant t \leqslant t_{k+1}^-$, where t_{k+1} denotes the instant where a new crack

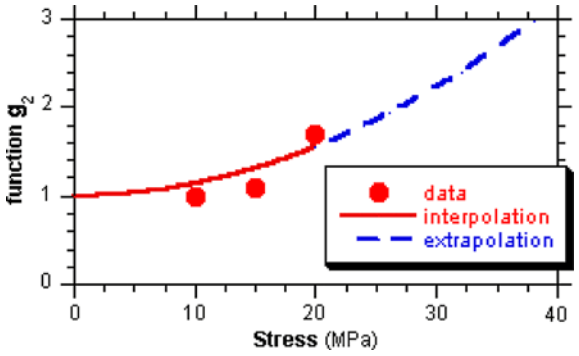

Fig. 8. Nonlinear function g_2 versus stress.

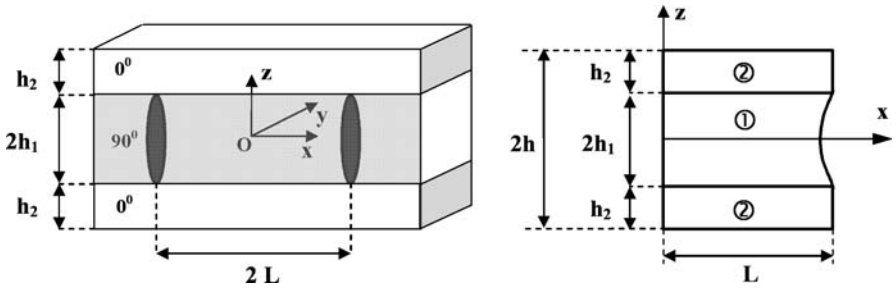

Fig. 9. Laminate and crack geometries.

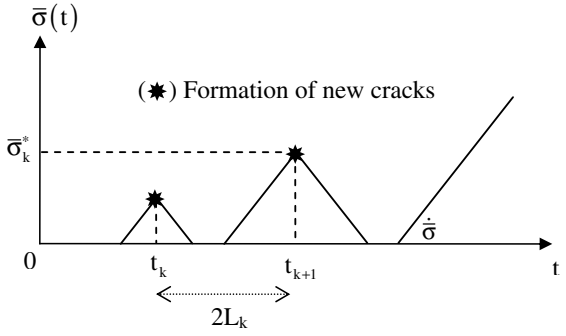

Fig. 10. "Ideal" progressive repeated loading program with hypothesis of new crack formations.

forms in the cell $2L_k$. Third, the nonlinear viscoelastic character will be taken into account but only the one-dimensional response of the laminate is considered. Let us also note that this cracking model is confined to a constant temperature condition (120 °C).

4.2. Mesoscale equations

The so-called mesoscale is defined as the scale of the ply – an intermediary between the microscale of the fibre and the macroscale of the laminate. Now, using Eq. (3) for the central 90°-layer of the laminate, the nonlinear viscoelastic constitutive equation in the x-direction using only one stress-dependent function g_2 is given in the form:

$$\varepsilon_x^{(1)}(x,z,t) = \frac{\partial U_1(x,z,t)}{\partial x} = J_{22}(t) \otimes \left[g_2\left(\sigma_{\text{eq}}\right) \sigma_x^{(1)}(x,z,t) \right] \quad (6)$$

where $\varepsilon_x^{(1)} = \varepsilon_x^{(1)}(x,z,t)$, $U_1 = U_1(x,z,t)$, $\sigma_x^{(1)} = \sigma_x^{(1)}(x,z,t)$ and $\tau_{xz}^{(1)} = \tau_{xz}^{(1)}(x,z,t)$ are respectively the strain, the displacement, the normal stress and the shear stress in the x-direction in the 90°-layer. All are functions of coordinates x, z and time t. The equivalent stress in the central layer is given by: $\sigma_{\text{eq}}(x,z,t) = \left[\sigma_x^{(1)2} + k_{\text{eq}}\tau_{xz}^{(1)2}\right]^{1/2}$, $k_{\text{eq}} \approx 3.03$ is taken as a suitable approximation for the material at hand [12]. Let now $\tilde{f}^{(1)}(\cdots) = \frac{1}{2h_1}\int_{-h_1}^{+h_1} f^{(1)}(\ldots,z)\,\mathrm{d}z$ and $\tilde{f}^{(2)}(\cdots) = \frac{1}{h_2}\int_{h_1}^{h_1+h_2} f^{(2)}(\ldots,z)\,\mathrm{d}z$ define the average values of any function f over the central layer thickness $2h_1$ and the outer layer thickness h_2, respectively. Averaging Eq. (6) over the thickness of the central layer amounts to eliminate the z-coordinate and results in:

$$\tilde{\varepsilon}_x^{(1)}(x,t) = \frac{\partial \tilde{U}_1(x,t)}{\partial x} = J_{22}(t) \otimes \left\langle g_2\left(\sigma_{\text{eq}}\right)\sigma_x^{(1)}(x,z,t)\right\rangle_{2h_1}$$

where the symbol $\langle\,\rangle_{2h_1}$ denotes the average of a particular function over the thickness of the central layer. By using the following approximation (see Appendix):

$$\left\langle \sigma_x^{(1)} g_2\left(\sigma_{\text{eq}}\right)\right\rangle_{2h_1} \approx \tilde{\sigma}_x^{(1)} g_2\left(\tilde{\sigma}_x^{(1)}\right) \quad (7)$$

the averaged constitutive equation of the layer can be obtained in the form:

$$\tilde{\varepsilon}_x^{(1)}(x,t) = \frac{\partial \tilde{U}_1(x,t)}{\partial x} = J_{22}(t) \otimes \left[\tilde{\sigma}_x^{(1)} g_2\left(\tilde{\sigma}_x^{(1)}\right)\right] \quad (8)$$

The outer 0°-layers are supposed to display an elastic behaviour in the x-direction. Their averaged constitutive equation has the form:

$$\tilde{\varepsilon}_x^{(2)}(x,t) = \frac{\partial \tilde{U}_2(x,t)}{\partial x} = \frac{1}{E_{11}}\tilde{\sigma}_x^{(2)}(x,t) \quad (9)$$

where $\tilde{\varepsilon}_x^{(2)}$, $\tilde{U}_2$, $\tilde{\sigma}_x^{(2)}$ are respectively the x-direction strain, displacement and normal stress averaged over the thickness of the 0°-layer.

With a view to applying the nonlinear correspondence principle, the behaviour of the interface between the outer 0°-layer and the central 90°-layer is supposed to result from the viscoelastic shear behaviour of the sole 90°-layer at $z = h_1$; for the material system at hand, taking into account the fact that (see Appendix):

$$\tau^* g_2\left(\sigma_{\text{eq}}^*\right) \approx \tau^* g_2\left(\tau^*\sqrt{k_{\text{eq}}}\right) \quad (10)$$

the interface constitutive behaviour can be obtained in the form:

$$\gamma^*(x,t) = J_{23}(t) \otimes \left[\tau^* g_2\left(\tau^*\sqrt{k_{\text{eq}}}\right)\right] \quad (11)$$

where the superscript $(^*)$ is used to denote the value of a variable at the interface $z = h_1$; $\gamma^* = \gamma_{xz}^{(1)}(x, z = h_1, t)$ is the shear strain related to the interfacial shear stress $\tau^* = \tau_{xz}^{(1)}(x, z = h_1, t)$; $J_{23}(t)$ is the shear creep function such that $J_{23}(t) = 2(1+\nu_{23})J_{22}(t)$, ν_{23} being out-of-plane Poisson's ratio which is supposed constant in this study ($\nu_{23} = 0.4$); $\sigma_{\text{eq}}^* = \sigma_{\text{eq}}(x, z = h_1, t)$ denotes the equivalent stress at the interface.

The displacements in the x-direction of the 90° and 0° layers, denoted by $U_1$and U_2 respectively, are assumed to have the following distribution:

$$\begin{cases} U_1(x,z,t) = z^2 f_1(x,t) + f_2(x,t), & |z| \leqslant h_1 \\ U_2(x,z,t) = \tilde{U}_2(x,t), & h_1 \leqslant |z| \leqslant h_1 + h_2 \end{cases} \tag{12}$$

where f_1 and f_2 are functions of the x-coordinate and time t. Supposing that the displacement in z-direction in the central layer varies very slowly with x, the following relation between the interface shear strain and the average displacements can be obtained by using the continuity condition for displacements at the interface (see the Appendix for details):

$$\gamma^*(x,t) = 3\frac{\tilde{U}_2(x,t) - \tilde{U}_1(x,t)}{h_1} \tag{13}$$

The averaged equilibrium equations of the layers and of the whole laminate are given by (see the Appendix for details):

$$h_1 \frac{\partial \tilde{\sigma}_x^{(1)}}{\partial x}(x,t) + \tau^*(x,t) = 0 \tag{14}$$

$$h_2 \frac{\partial \tilde{\sigma}_x^{(2)}}{\partial x}(x,t) - \tau^*(x,t) = 0 \tag{15}$$

$$h_1 \tilde{\sigma}_x^{(1)}(x,t) + h_2 \tilde{\sigma}_x^{(2)}(x,t) = (h_1 + h_2)\bar{\sigma}(t) \tag{16}$$

The boundary conditions, at $x = 0$ and $x = L$, appropriate to the geometry of the cracked laminate shown in Fig. 8, are given by:

$$\tilde{\sigma}_x^{(1)}(L,t) = 0; \quad \tau^*(0,t) = 0 \tag{17}$$

The eight unknowns ($\tilde{\sigma}_x^{(1)}$, $\tilde{\sigma}_x^{(2)}$, τ^*, $\tilde{\varepsilon}_x^{(1)}$, $\tilde{\varepsilon}_x^{(2)}$, γ^*, $\tilde{U}_1$, $\tilde{U}_2$) of the viscoelastic problem are the solution of the system of Eqs. (8), (9), (11), (13)–(16) with boundary conditions (17) and suitable initial conditions.

4.3. Matrix cracking development

4.3.1. Nonlinear correspondence principle

In this sub-section, the nonlinear correspondence principle [13] is used to find an approximate solution of the above nonlinear viscoelastic problem by introducing a "reference" elastic problem. Once the reference elastic solution is found, the viscoelastic solution can be computed by using simple relationships between the two solutions.

The so-called correspondence principle used here is not the classical correspondence principle, which supposes a linear behaviour, but the very special "nonlinear correspondence principle" introduced by R.A. Schapery, which allows the nonlinear viscoelastic problem to be replaced by a nonlinear elastic problem.

The creep function found in the preceding section can be rewritten in the form: $J_{22}(t) = J_{20}D(t)$, where $D(t)$ is a dimensionless function, whose value is always close to unity (Fig. 11), such that:

$$D(t) = 1 + \Delta D(t), \quad \Delta D(t) = \sum_{n=1}^{3} \frac{J_{2n}}{J_{20}}(1 - e^{-t}/\tau_n) \tag{18}$$

The averaged constitutive equation of the 90°-layer, given by Eq. (8), is rewritten in the form:

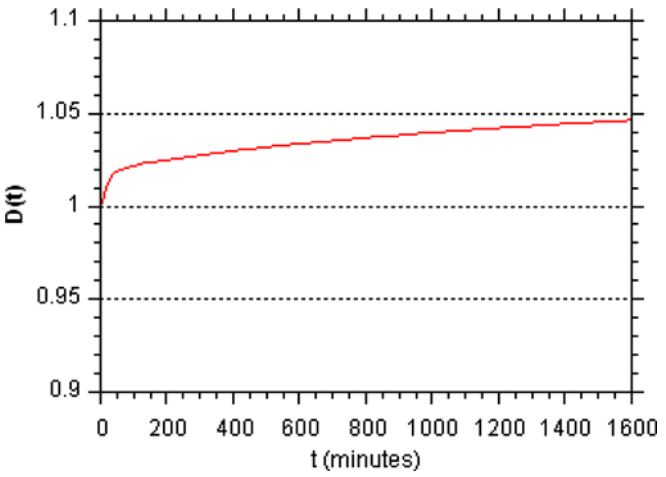

Fig. 11. Variation of the function $D(t)$ for carbon/epoxy IM7/977-2 at 120 °C.

$$\tilde{\varepsilon}_x^{(1)}(x,t) = D(t) \otimes \left[J_{20}\tilde{\sigma}_x^{(1)} g_2\left(\tilde{\sigma}_x^{(1)}\right)\right] \tag{19}$$

In order to apply the nonlinear correspondence principle, the outer 0°-layers are artificially supposed to display a "viscoelastic" behaviour in the x-direction by using the following approximation:

$$\tilde{\varepsilon}_x^{(2)}(x,t) = \frac{1}{E_{11}}\tilde{\sigma}_x^{(2)}(x,t) \approx D(t) \otimes \left[\frac{1}{E_{11}}\tilde{\sigma}_x^{(2)}(x,t)\right] \tag{20}$$

The constitutive equation of the interface, Eq. (11), can be rewritten in a form involving the same function D(t):

$$\gamma^*(x,t) = D(t) \otimes \left[2(1+\nu_{23})J_{20} g_2\left(\sigma_{\text{eq}}^*\right)\tau^*(x,t)\right] \tag{21}$$

Now, a "reference" elastic problem, with the same traction boundary conditions as those of the viscoelastic problem, is defined by new unknown functions denoted by superscript "R" such that:

$$\tilde{\sigma}_x^{(i)}(x,t) = \tilde{\sigma}_x^{(i)\mathrm{R}}(x,t), \quad i = 1,2 \tag{22}$$

$$\tau^*(x,t) = \tau^{*\mathrm{R}}(x,t) \tag{23}$$

$$\tilde{\varepsilon}_x^{(i)}(x,t) = D(t) \otimes \tilde{\varepsilon}_x^{(i)\mathrm{R}}(x,t), \quad i = 1,2 \tag{24}$$

$$\gamma^*(x,t) = D(t) \otimes \gamma^{*\mathrm{R}}(x,t) \tag{25}$$

$$\tilde{\varepsilon}_x^{(i)\mathrm{R}}(x,t) = \frac{\partial \tilde{U}_i^{\mathrm{R}}(x,t)}{\partial x}, \quad i = 1,2 \tag{26}$$

$$\gamma^{*\mathrm{R}}(x,t) = 3\frac{\tilde{U}_2^{\mathrm{R}}(x,t) - \tilde{U}_1^{\mathrm{R}}(x,t)}{h_1} \tag{27}$$

Substituting Eqs. (22)–(27) into the corresponding viscoelastic equations derived in the preceding section leads to the constitutive equations of the layers and the interface of the "R" problem in the form:

$$\tilde{\varepsilon}_x^{(1)\mathrm{R}}(x,t) = J_{20}\left[\tilde{\sigma}_x^{(1)\mathrm{R}}(x,t) g_2\left(\tilde{\sigma}_x^{(1)\mathrm{R}}(x,t)\right)\right] \tag{28}$$

$$\tilde{\varepsilon}_x^{(2)\mathrm{R}}(x,t) = \frac{1}{E_{11}}\tilde{\sigma}_x^{(2)\mathrm{R}}(x,t) \tag{29}$$

$$\gamma^{*\mathrm{R}}(x,t) = 2(1+\nu_{23})J_{20}\left[\tau^{*\mathrm{R}}(x,t) g_2\left(\tau^{*\mathrm{R}}(x,t)\sqrt{k_{\text{eq}}}\right)\right] \tag{30}$$

It can be seen that the R-unknowns are the solution of a nonlinear elastic problem.

Next, using the relationship between the interface shear strain and the average displacements of the reference elastic problem given by Eq. (27), then eliminating the strain variables by using Eqs. (26) and (28)–(30), results in the following relationship only involving the R-stresses:

$$\frac{\partial \tau^{*\mathrm{R}}}{\partial x} - \frac{1}{\frac{\partial}{\partial \tau^{*\mathrm{R}}}\left[\frac{2h_1}{3}(1+v_{23})\tau^{*\mathrm{R}} g_2\left(\tau^{*\mathrm{R}}\sqrt{k_{\mathrm{eq}}}\right)\right]} \times \left\{\frac{J_{11}}{J_{20}}\tilde{\sigma}_{\mathrm{x}}^{(2)\mathrm{R}} - \tilde{\sigma}_x^{(1)\mathrm{R}} g_2\left(\tilde{\sigma}_x^{(1)\mathrm{R}}\right)\right\} = 0 \tag{31}$$

Note that as the stresses are the same for both problems, all the relations between viscoelastic stresses are equally valid for the elastic stresses denoted by superscript "R". Therefore the equilibrium equations of the layers of the reference elastic problem are given by:

$$\frac{\partial \tilde{\sigma}_x^{(1)\mathrm{R}}}{\partial x} + \frac{\tau^{*\mathrm{R}}}{h_1} = 0 \tag{32}$$

$$\frac{\partial \tilde{\sigma}_x^{(2)\mathrm{R}}}{\partial x} - \frac{\tau^{*\mathrm{R}}}{h_2} = 0 \tag{33}$$

The averaged boundary conditions at $x = 0$ and $x = L$ are:

$$\tilde{\sigma}_x^{(1)\mathrm{R}}(L,t) = 0; \quad \tilde{\sigma}_x^{(2)\mathrm{R}}(L,t) = (1+h_{12})\bar{\sigma}(t); \quad \tau^{*\mathrm{R}}(0,t) = 0 \tag{34}$$

Now the set of nonlinear ordinary differential equations (31)–(33) with the boundary conditions equation (34) can be used to compute the "R" elastic stresses ($\tilde{\sigma}_x^{(1)\mathrm{R}}$, $\tilde{\sigma}_x^{(2)\mathrm{R}}$ and $\tau^{*\mathrm{R}}$). In this new problem, time t only acts as a parameter through the prescribed laminate stress $\bar{\sigma}(t)$. Once the "R" elastic stresses are found, the nonlinear viscoelastic stresses and strains are obtained by using the viscoelastic–elastic relationships equations (22)–(25). Then, a failure criterion must be used to describe the cracking evolution.

4.3.2. Failure criteria

A critical strain failure criterion will be used here to predict crack multiplication as a function of applied load level. This criterion states that a new crack appears in the central 90°-layer when the maximum strain attains some critical value. In order to study the loading rate effect on cracking, two versions of the criterion will be considered. If the critical value is a constant and does not depend upon the loading rate, the criterion is called "rate insensitive", which reads:

$$\max_{-L\leqslant x\leqslant L}\left[\tilde{\varepsilon}_x^{(1)}(x,t)\right] = \varepsilon_{\mathrm{c}} \tag{35}$$

If the critical value depends on the loading rate, we have a so-called "rate sensitive" criterion which can be expressed in the following form:

$$\max_{-L\leqslant x\leqslant L}\left[\tilde{\varepsilon}_x^{(1)}(x,t)\right] = \varepsilon_{\mathrm{c}} + k_{\varepsilon}(\dot{\bar{\sigma}}/\dot{\bar{\sigma}}_{\mathrm{r}})^n \tag{36}$$

where ε_{c}, k_{ε}, n are material constants and $\dot{\bar{\sigma}}_{\mathrm{r}}$ denotes a reference stress rate. For the sake of presentation, $\varepsilon_{\mathrm{c}}^{(1)}(\dot{\bar{\sigma}})$ will denote the general expression of the critical value in the two cases. Other failure criteria (such as a maximum stress criterion or Reiner-Weissenberg free energy density criterion), have been attempted and compared [6].

4.4. Numerical approach and results

A numerical program using the shooting method [14] was developed to solve the system of nonlinear differential equations (31)–(33), with the non homogenous boundary conditions equation (34). The unknowns are the "R" elastic stresses consisting of the average normal stresses $\tilde{\sigma}_x^{(i)\mathrm{R}}$ in layers i ($i = 1, 2$) and the interface shear stress $\tau^{*\mathrm{R}}$. For a given damage state characterized by the half distance $L = L_k$ between two adjacent cracks, at any applied load level $\bar{\sigma}(t)$, the stress distribution between the cracks can be obtained. With the above-mentioned imposed boundary conditions, the average normal stress in the 90°-layer ($\tilde{\sigma}_x^{(1)\mathrm{R}}$) in x-direction is found to reach its maximum value midway between cracks ($x = 0$).

A critical strain failure criterion is then used to obtain a numerical simulation of the crack density as a function of the applied stress. Using Eq. (24), the relationship between the viscoelastic and "R" elastic strains in the 90°-layer, at time $t = t_j$, can be obtained in the form:

$$\tilde{\varepsilon}_x^{(1)}(x,t_j) = \int_0^{t_j} D(t_j - t')\frac{\partial\left[\tilde{\varepsilon}_x^{(1)\mathrm{R}}(x,t')\right]}{\partial t'}\mathrm{d}t' \quad (-L\leqslant x\leqslant L) \tag{37}$$

Taking into account the monotonic loading history $\bar{\sigma}(t) = \dot{\bar{\sigma}}(t), \dot{\bar{\sigma}}$ being the constant loading rate, leads to:

$$\tilde{\varepsilon}_x^{(1)}\left(x,\bar{\sigma}_j\right) = \int_0^{\bar{\sigma}_j} D\left(\frac{\bar{\sigma}_j}{\dot{\bar{\sigma}}} - \frac{\sigma'}{\dot{\bar{\sigma}}}\right)\frac{\partial\left[\tilde{\varepsilon}_{\mathrm{x}}^{(1)\mathrm{R}}(x,\sigma')\right]}{\partial\sigma'}\mathrm{d}\sigma' \tag{38}$$

where $\bar{\sigma}_j = \dot{\bar{\sigma}}t_j$. For the sake of convenience, let us set $\tilde{\varepsilon}_j = \tilde{\varepsilon}_x^{(1)}\left(x,\bar{\sigma}_j\right)$ and $\tilde{\varepsilon}_j^{\mathrm{R}} = \tilde{\varepsilon}_{\mathrm{x}}^{(1)\mathrm{R}}\left(x,\bar{\sigma}_j\right)$. Using Eq. (18), Eq. (38) can be rewritten in a form involving the function $\Delta D(t)$:

$$\tilde{\varepsilon}_j = \tilde{\varepsilon}_j^{\mathrm{R}} + \int_0^{\bar{\sigma}_j}\Delta D\left(\frac{\bar{\sigma}_j}{\dot{\bar{\sigma}}} - \frac{\sigma'}{\dot{\bar{\sigma}}}\right)\frac{\partial}{\partial\sigma'}\left[\tilde{\varepsilon}_j^{\mathrm{R}}\right]\mathrm{d}\sigma' \tag{39}$$

In (39) the first "elastic" term $\tilde{\varepsilon}_j^{\mathrm{R}}$ can easily be evaluated by using Eq. (28). In order to calculate the second term involving the integral, one can assume that $\tilde{\varepsilon}_j^{\mathrm{R}}$ varies linearly during each stress increment $\Delta\bar{\sigma}$ such that $\bar{\sigma}_j = N_j\Delta\bar{\sigma}$, N_j being a large integer; then Eq. (39) is approximated by:

$$\tilde{\varepsilon}_j = \tilde{\varepsilon}_j^{\mathrm{R}} + \sum_{i=1}^{i=N_j}\left[\frac{\tilde{\varepsilon}_i^{\mathrm{R}} - \tilde{\varepsilon}_{i-1}^{\mathrm{R}}}{\Delta\bar{\sigma}}\int_{(i-1)\Delta\bar{\sigma}}^{i\Delta\bar{\sigma}}\Delta D\left(\frac{N_j\Delta\bar{\sigma}}{\dot{\bar{\sigma}}} - \frac{\sigma'}{\dot{\bar{\sigma}}}\right)\mathrm{d}\sigma'\right] \tag{40}$$

where $\tilde{\varepsilon}_i = \tilde{\varepsilon}_x^{(1)}(x,\bar{\sigma}_i = i\Delta\bar{\sigma})$ and $\tilde{\varepsilon}_i^{\mathrm{R}} = \tilde{\varepsilon}_{\mathrm{x}}^{(1)\mathrm{R}}(x,\bar{\sigma}_i = i\Delta\bar{\sigma})$. The expression (40) can be evaluated at any position x between two adjacent cracks spaced $2L$ apart ($-L \leqslant x \leqslant L$).

At a given damage state (namely for a fixed value of L_k or a fixed crack density ρ_k, $\rho_k = 1/(2L_k)$), the normal stress in the 90°-layer takes its maximum midway between two adjacent cracks ($x = 0$). Then the strain in the layer reaches its maximum at $x = 0$ because all the strains go back to zero everywhere in the layer at the end of each loading "cycle" of the "ideal" progressive repeated loading pro-

gram (Fig. 10). When the applied stress varies from $\bar{\sigma} = 0$ to $\bar{\sigma} = \bar{\sigma}_j$, the maximum viscoelastic strain $\tilde{\varepsilon}_j^{\max} = \tilde{\varepsilon}_x^{(1)}(x = 0, \bar{\sigma}_j)$ is computed by applying Eq. (40) at $x = 0$; then it is checked whether $\tilde{\varepsilon}_j^{\max}$ equals the critical value $\varepsilon_c^{(1)}$; if this failure condition is satisfied, the values of the applied stress $\bar{\sigma}_j = \bar{\sigma}_k^*$ and of the corresponding crack density ρ_k are saved; otherwise, the applied stress is further increased until the criterion is met; the stress increment should be small enough to obtain a correct value of $\bar{\sigma}_k^*$. This calculation procedure is repeated for several L_k values in order to find the stress $\bar{\sigma}_k^*$ at which a new crack forms (a cracking curve is thus obtained). Note that the applied stress starts from zero (then increases to $\bar{\sigma}_k^*$) for each calculation involving a new L_k value.

Fig. 12 presents the numerical simulation of the variation of the maximum normal stress (at $x = 0$) when the applied stress increases, for a fixed value of crack density. In the figure, the "linear stress" obtained by taking $g_2 = 1$ and the so-called "effective stress" defined by $\tilde{\sigma}_{\text{eff}}^{(1)} = \tilde{\sigma}_{\text{x}}^{(1)\text{R}} \times g_2(\tilde{\sigma}_x^{(1)\text{R}}) = \tilde{\sigma}_x^{(1)} \times g_2(\tilde{\sigma}_x^{(1)})$ are also plotted; this "effective stress" appearing in Eq. (28) "governs" the variation of the "R" nonlinear elastic strain $\tilde{\varepsilon}_x^{(1)\text{R}}$.

Fig. 13 presents the variation of the maximum nonlinear viscoelastic strain in the 90°-layer with the applied stress for the three considered loading rates. Fig. 14 presents the predicted crack evolution obtained from a maximum strain failure criterion whose critical value is independent of the loading rate. It can be seen on the zoomed-in figure that, for the three considered loading rates, the numerically predicted cracking curves are very close from each other.

Therefore, the rate-insensitive version of the failure criterion Eq. (35) cannot adequately display the effect of the loading rate on the experimental cracking curves. On the other hand, it can be seen that the values of constants k_ε and n in a criterion of the type Eq. (36) convey the loading rate sensitivity of the simulated cracking curves. Fig. 15 presents the numerically simulated evolution of the crack density for the three loading rates, obtained by using a rate-dependent critical strain failure criterion with the following material constants: $\varepsilon_c = 0.0058$, $k_\varepsilon = 0.0012$ and $n = 0.23$; $\dot{\bar{\sigma}}_r = 1.3216$ MPa/min. The predicted curves obtained from the 1D linear viscoelastic analysis detailed in [6] (again using a shear-lag approach) are also presented in the figure together with the experimental data.

Note that the stress increment $\Delta\bar{\sigma}$ is 2.5 MPa for all simulations presented in Figs. 12–15; another simulation using a smaller stress increment, $\Delta\bar{\sigma} = 1$ MPa, brought no significant improvement.

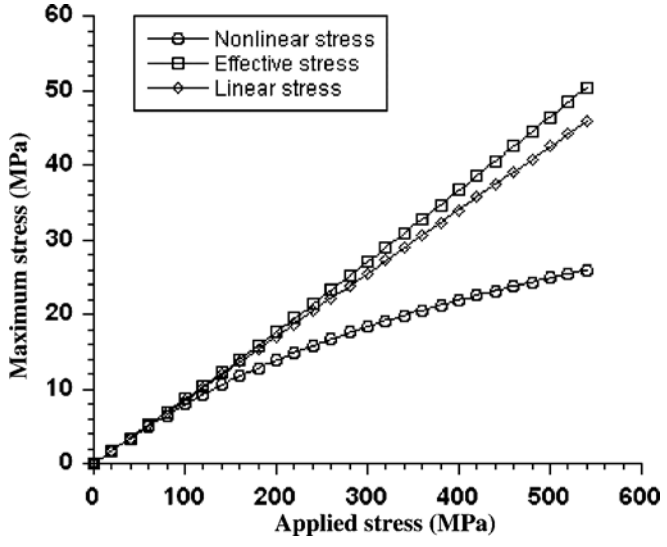

Fig. 12. Variation of maximum stress (MPa) between two adjacent cracks in the 90°-layer as a function of applied stress (MPa), obtained when the crack density equals 5 (cm^{-1}).

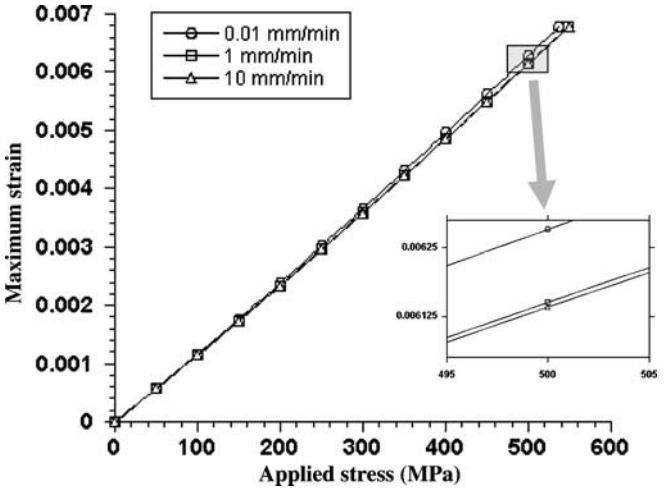

Fig. 13. Influence of the loading rate on the evolution of the maximum nonlinear viscoelastic strain between two adjacent cracks in the central 90°-layer, obtained when the crack density equals 5 (cm^{-1}); $[0_3/90_3]_S$ IM7/977-2 laminate.

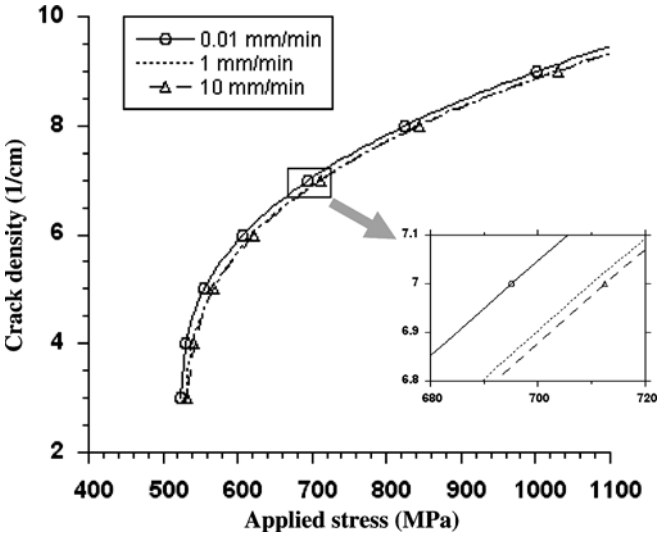

Fig. 14. Predicted transverse cracking evolution at 120 °C for three loading rates using a rate-independent critical strain criterion ($\varepsilon_c = 0.007$); $[0_3/90_3]_S$ IM7/977-2 laminate.

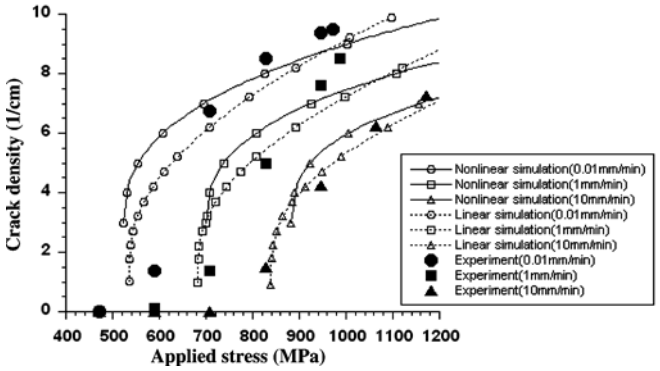

Fig. 15. Crack density (cm^{-1}) versus applied stress (MPa) at 120 °C for three loading rates. Comparison between experiment, 1D viscoelastic linear [6] and nonlinear simulations using a rate-dependent critical strain criterion ($\varepsilon_c = 0.0058$, $k_\varepsilon = 0.0012$ and $n = 0.23$). $[0_3/90_3]_S$ IM7/977-2 laminate.

5. Discussion and conclusions

The monotonic tensile tests performed on the IM7/977-2 carbon/epoxy $[0_3/90_3]_S$ laminates at 120 °C, with three respective crosshead velocities (0.01 mm/min, 1 mm/min and 10 mm/min), have displayed a marked loading rate dependence of the transverse matrix cracking evolution. Several phenomena might explain this effect: the viscoelastic behaviour of the undamaged material in the 90°-plies and that of the damaged material surrounding the crack front. The above effect could also be connected with thermal, physical and chemical ageing processes in the material.

5.1. Influence of viscoelastic behaviour (linear and nonlinear) of the undamaged material

The 1D and 2D linear viscoelastic analyses, detailed in our previous papers [6,7], have shown that the linear viscoelastic character of the undamaged material is not marked enough to explain alone the influence of the loading rate on the cracking process for the material at hand.

The aim of the present paper was to assess a possible effect on the phenomenon of the nonlinear viscoelastic behaviour of the undamaged material in the 90°-plies. A material characterization procedure using a simplified Schapery model was proposed in Section 3 in order to identify the nonlinear viscoelastic constitutive equation of the 90°-layer by using data obtained from the creep-recovery tests. The damage analysis was carried out in Section 4 to numerically predict the cracking evolution as a function of the applied load by using two versions of a strain failure criterion. Some stringent simplifying assumptions were used insofar as our main objective was to investigate the impact of any nonlinear material behaviour on loading rate sensitivity of the cracking process.

The comparison between the linear and nonlinear stress responses when the crack density ρ equals 5 cm^{-1}, presented in Fig. 12, shows that the material nonlinearity, described by the nonlinearizing function $g_2(\sigma)$, sharply decreases the stress level between two existing cracks in the damaged 90°-layer. However, the nonlinear strain is related with the "effective stress" which is greater than the "linear stress" as presented in Fig. 12; so that, at this damage state ($\rho = 5\ cm^{-1}$), using a strain failure criterion, the "nonlinear simulation" predicts an earlier cracking process than the "linear simulation" (as shown in Fig. 15).

Fig. 13 presents the predicted variation of the maximum strain between two adjacent cracks in the 90°-layer with the applied stress for three loading rates. It can be seen that the slopes of the simulated curves are slightly different, which means that, for the material at hand, there is a weak influence of the loading rate due to the nonlinear viscoelastic behaviour of the material. As a result, the rate insensitive failure criterion given by Eq. (35), in which the critical value is a constant, cannot sufficiently convey the influence of the loading rate on the experimental cracking curves; the predicted cracking curves obtained for the three loading rates (Fig. 14) are too close from each other. A supplementary simulation with an "artificially enhanced" nonlinearity using the function $g_2(\sigma) = 1 + ca_g\sigma^{b_g}$, with $c = 5$, did not show a noticeable increase in the loading rate sensitivity of the cracking curves.

5.2. Influence of the viscoelastic behaviour of the damaged material

The viscoelastic behaviour of the undamaged material cannot alone explain the marked effect of the loading rate on transverse cracking. On the other hand, the rate sensitive failure criterion, expressed by Eq. (36), gives a good agreement between the experimental data and the simulated cracking curves displayed in Fig. 15. Using a rate-dependent critical value amounts to take into account the viscoelastic character of the failing material in the process zone around crack fronts. Moreover, another cracking test, at 120 °C under neutral environment (nitrogen), with a loading rate of 13.216 MPa/min (corresponding to a crosshead velocity of 0.1 mm/min) has shown that the possible oxidation of the material had no effect on the loading rate sensitivity of the cracking process [15].

5.3. Improvement of the cracking description

As shown in Fig. 15, the predicted cracking curves, for each loading rate, are in good agreement with experiment except for the very early phase of the phenomenon. A probabilistic energy based criterion proposed by Vinogradov and Hashin [16] can be attempted in order to better reproduce the S-form of the cracking curves by properly describing the very low crack density range. In fact, using this approach [16] amounts to take into account the "R-curve" effect when characterizing the resistance to transverse crack multiplication, as empirically showed by Han et al. [17].

For the material system at hand, the numerical simulations have showed that the viscoelastic behaviour (linear or nonlinear) of the undamaged material cannot explain

the marked effect of the loading rate on transverse cracking. On the other hand, the loading rate dependence of the critical material strength gives a good description of the phenomenon. Therefore, the cracking process can be sufficiently well described by assuming a linear elastic behaviour for the undamaged material and using a failure criterion involving a rate-dependent critical value displaying a "R-curve" effect. An energy balance based criterion can be written in the form:

$$G(\bar{\sigma},\rho)=\gamma(\rho,\dot{\bar{\sigma}}) \tag{41}$$

The elastic energy release rate G [17] in the left-hand side of Eq. (41), which is found by using a 1D shear-lag stress analysis [17,18] and by supposing that new cracks appear midway between two existing adjacent cracks, assuming a $2L$ uniform spacing ($L=1/(2\rho)$, ρ being the crack density), is in the form:

$$G(\bar{\sigma},\rho)=G_{\max}(\bar{\sigma})\left\{\tanh\left(\frac{\alpha}{2\rho}\right)-\frac{\alpha}{2\rho}\left[1-\tanh^2\left(\frac{\alpha}{2\rho}\right)\right]\right\} \tag{42}$$

where $G_{\max}(\bar{\sigma})=\frac{1}{\alpha}\frac{E_{22}}{E_x}\frac{1}{E_{11}}(1+h_{12})\left[\bar{\sigma}-\frac{1}{(1+h_{12})}E_{11}\Delta\alpha_{21}\Delta T\right]^2$; $E_x=\frac{E_{11}+h_{12}E_{22}}{1+h_{12}}$; $\Delta\alpha_{21}=\alpha_2-\alpha_1$; $h_{12}=h_1/h_2$; $\alpha^2=\frac{3G_{23}}{h_1}\times\left(\frac{1}{h_2E_{11}}+\frac{1}{h_1E_{22}}\right)$. A 2D analysis can also be derived [19]. The critical energy release rate γ is assumed to be a function of both crack density ρ and loading rate $\dot{\bar{\sigma}}$ in the form:

$$\gamma(\rho,\dot{\bar{\sigma}})=\gamma_0+(m_0+m_1\rho^{m_2})\left(\frac{\dot{\bar{\sigma}}}{\dot{\bar{\sigma}}_r}\right)^{m_3} \tag{43}$$

where m_0, m_1, m_2, m_3 are material constants and $\dot{\bar{\sigma}}_r$ denotes a reference stress rate; $(m_0+\gamma_0)$ is the "initial" value of the critical energy release rate corresponding to cracking onset when $\dot{\bar{\sigma}}=\dot{\bar{\sigma}}_r$. For a given loading rate, γ increases as the crack density increases ("R-curve" effect). Fig. 16 represents the simulated cracking curves obtained for the three loading rates, by using the law (43) with the constants: $\gamma_0=157.2$ (J/m^2), $m_0=0$ J/m^2, $m_1=57.6$ (J/m^2), $m_2=0.256$, $m_3=0.2$ and $\dot{\bar{\sigma}}_r=1.3216$ MPa/min. A good agreement between the experimental data [4] and the proposed simulation has been obtained regarding both the rate sensitivity and the S-form of the cracking curves for each loading rate. It can also be seen in Fig. 16 that the slopes of the simulated cracking curves are very different for the three studied loading rates. This can be "explained" by taking into account both the "R-curve" effect and the loading rate dependence of the critical value, γ, of energy release rate in the form of Eq. (43).

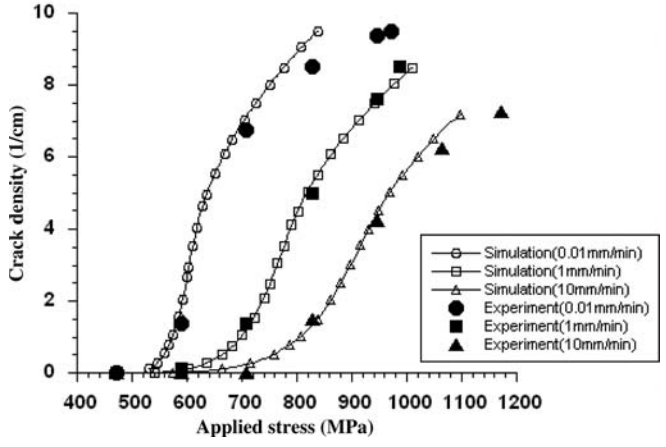

Fig. 16. Crack density (cm^{-1}) versus applied stress (MPa) at 120 °C for three loading rates. Comparison between experiment and simulations using an energy based criterion involving both "R-effect" and loading rate effect into critical value. $[0_3/90_3]_S$ IM7/977-2 laminate.

5.4. Prospects

The rate dependence of the material resistance to transverse matrix cracking (at the studied temperature of 120 °C) was described in a phenomenological way. It is known that the toughness of the material is the area of the "traction-separation curve" $\sigma(\delta,\dot{\delta})$ pertaining to the cohesive zone ahead of the crack front, where the local stress σ depends upon the crack opening displacement δ and its opening rate $\dot{\delta}$; see Landis et al. [20] for example. In order to predict the traction-separation law, it would be desirable to be able to deduce the behaviour of the failing material in the cohesive zone from that of the bulk material. However this problem is still widely open, excepting for some works dealing with polymer fracture [21].

Until now we have supposed that the new cracks immediately cross the specimen width as they appear. In order to better assess the loading rate influence on the phenomenon, it would be advisable to take into account the finite time of propagation of matrix cracks in the width direction of the specimen. A possible approach could use the work of Liang et al. [22,23].

One of the most important conclusions of this work is that, though important, the nonlinearity of the undamaged material does not significantly enhance the stress (or strain) rate sensitivity of the damaging process.

Acknowledgments

The authors gratefully acknowledge J.M. Lebeau for the cracking tests conducted during his Master project under the supervision of Professor M.C. Lafarie-Frenot at Laboratoire de Mécanique et de Physique des Matériaux (L.M.P.M.). The authors thank A. Vinet (CCR-EADS, France) for the experimental data of the creep-recovery tests. They are indebted to Professor M.C. Lafarie-Frenot for worthy advice and discussion on the subject.

Appendix A. Approximations (7) and (10)

In this section, the approximations given by (7) and (10) are assessed in the case when the outer 0°-layers and the inner 90°-layer are supposed to display a linear elastic behaviour in the x-direction. A 1D stress state is considered in this analysis based on a shear-lag approach [17,18].

A.1. Stress analysis

The constitutive equations of the layers and of the interface are:

$$\varepsilon_x^{(1)}(x,z) = \frac{\partial U_1(x,z)}{\partial x} = \frac{1}{E_{22}}\sigma_x^{(1)}(x,z) \tag{A.1}$$

$$\varepsilon_x^{(2)}(x,z) = \frac{\partial U_2(x,z)}{\partial x} = \frac{1}{E_{11}}\sigma_x^{(2)}(x,z) \tag{A.2}$$

$$\gamma^*(x) = \frac{1}{G_{23}}\tau^*(x) \tag{A.3}$$

where E_{11}, E_{22}, G_{23} are respectively the longitudinal, transverse and shear modulus of the unidirectional ply given in Table 1; $\gamma^*(x) = \gamma_{xz}^{(1)}(x, z = h_1)$ is the shear strain related to the interfacial shear stress $\tau^*(x) = \tau_{xz}^{(1)}(x, z = h_1)$. Averaging Eqs. (A.1) and (A.2) over the thickness of the 90°-layer and the 0°-layer, respectively, results in the averaged constitutive equations of the layers as follows:

$$\tilde{\varepsilon}_x^{(1)}(x) = \tilde{U}_1'(x) = \frac{1}{E_{22}}\tilde{\sigma}_{\mathrm{x}}^{(1)}(x) \tag{A.4}$$

$$\tilde{\varepsilon}_x^{(2)}(x) = \tilde{U}_2'(x) = \frac{1}{E_{11}}\tilde{\sigma}_{\mathrm{x}}^{(2)}(x) \tag{A.5}$$

The prime symbol denotes a derivative with respect to x. The displacement distributions in the x-direction in the layers are assumed as follows:

$$\begin{cases} U_1(x,z) = z^2 f_1(x) + f_2(x), & |z| \leqslant h_1 \\ U_2(x,z) = \tilde{U}_2(x), & h_1 \leqslant |z| \leqslant h_1 + h_2 \end{cases} \tag{A.6}$$

From the definition of $\tilde{U}_1$ and the continuity condition for displacements at the interface ($z = h_1$), the two space functions $f_1(x)$ and $f_2(x)$ can be expressed as:

$$\begin{cases} f_1(x) = \frac{3}{2h_1^2}\left[\tilde{U}_2(x) - \tilde{U}_1(x)\right] \\ f_2(x) = \frac{1}{2}\left[3\tilde{U}_1(x) - \tilde{U}_2(x)\right] \end{cases} \tag{A.7}$$

Supposing that the displacement in the z-direction in the 90°-layer varies very slowly with x, a relationship between the interfacial shear strain (γ^*) and the averaged displacements ($\tilde{U}_1, \tilde{U}_2$) can be obtained (in the same form as Eq. (15)); Then from Eq. (A.3), we obtain:

$$\tau^*(x) = \frac{3G_{23}}{h_1}\left[\tilde{U}_2(x) - \tilde{U}_1(x)\right] \tag{A.8}$$

Taking the derivative of Eq. (A.8) with respect to x results in:

$$\tilde{U}_2'(x) - \tilde{U}_1'(x) = \frac{h_1}{3G_{23}}\tau^{*\prime}(x) \tag{A.9}$$

Combining Eq. (A.9) with Eqs. (A.4) and (A.5) leads to the following ordinary differential equation:

$$\tau^{*\prime\prime}(x) - \alpha^2\tau^*(x) = 0 \tag{A.10}$$

where

$$\alpha^2 = \frac{3G_{23}}{h_1}\left[\frac{1}{h_2E_{11}} + \frac{1}{h_1E_{22}}\right]$$

Taking into account the boundary conditions at $x = 0$ and $x = L$ (Eq. (19)), the solution for the interface shear stress can be obtained as:

$$\tau^*(x) = \left[\frac{3G_{23}}{E_{11}}\frac{h}{h_1h_2}\bar{\sigma}\right]\frac{\sinh(\alpha x)}{\alpha\cosh(\alpha L)} \tag{A.11}$$

where $h = h_1 + h_2$.

Substituting Eq. (A.11) into Eq. (A.9) leads to:

$$\tilde{U}_2'(x) - \tilde{U}_1'(x) = \frac{1}{E_{11}}\frac{h}{h_2}\frac{\cosh(\alpha x)}{\cosh(\alpha L)}\bar{\sigma} \tag{A.12}$$

The averaged equilibrium equation of the 90°-layer is given by:

$$h_1\tilde{\sigma}_x^{(1)\prime}(x) + \tau^*(x) = 0 \tag{A.13}$$

Substituting Eq. (A.11) into Eq. (A.13), then integrating this equation and applying the boundary conditions, the solution for averaged normal stress in the 90°-layer is found in the form:

$$\tilde{\sigma}_x^{(1)}(x) = \frac{E_{22}}{E_x}\left(1 - \frac{\cosh(\alpha x)}{\cosh(\alpha L)}\right)\bar{\sigma} \tag{A.14}$$

where $E_x = \frac{h_1E_{22} + h_2E_{11}}{h}$. Combining Eqs. (A.14) and (A.12) leads to:

$$\tilde{U}_2'(x) - \tilde{U}_1'(x) = \frac{1}{E_{11}}\frac{h}{h_2}\left[\bar{\sigma} - \frac{E_{\mathrm{x}}}{E_{22}}\tilde{\sigma}_x^{(1)}(x)\right] \tag{A.15}$$

Substituting Eq. (A.15) into the derivative with respect to x of Eq. (A.7) results in:

$$f_1'(x) = \frac{3}{2h_1^2}\frac{1}{E_{11}}\frac{h}{h_2}\left[\bar{\sigma} - \frac{E_x}{E_{22}}\tilde{\sigma}_x^{(1)}(x)\right] \tag{A.16}$$

Substituting the displacement distribution in the 90°-layer given by Eq. (A.6) into Eq. (A.1) gives:

$$\sigma_x^{(1)}(x,z) = E_{22}\left[z^2f_1'(x) + f_2'(x)\right] \tag{A.17}$$

Integrating Eq. (A.17) over the thickness of the 90°-layer gives the averaged normal stress in the form:

$$\tilde{\sigma}_x^{(1)} = \frac{1}{h_1}\int_0^{h_1}\sigma_{\mathrm{x}}^{(1)}\mathrm{d}z = E_{22}\left[\frac{h_1^2}{3}f_1'(x) + f_2'(x)\right] \tag{A.18}$$

Eliminating $f_2'(x)$ from Eqs. (A.17) and (A.18) leads to:

$$\sigma_x^{(1)}(x,z) = \tilde{\sigma}_x^{(1)}(x) + E_{22}\left[z^2 - \frac{h_1^2}{3}\right]f_1'(x) \tag{A.19}$$

Substituting Eq. (A.16) into Eq. (A.19), results in the following relationship between the "local stress" $\sigma_x^{(1)}(x,z)$, the averaged stress $\tilde{\sigma}_x^{(1)}(x)$ and the applied stress $\bar{\sigma}$:

$$\sigma_x^{(1)}(x,z) = \tilde{\sigma}_x^{(1)}(x) + \frac{1}{2}\frac{h}{h_2}\frac{1}{E_{11}}\left[E_{22}\bar{\sigma} - E_x\tilde{\sigma}_x^{(1)}(x)\right]\left(\frac{3z^2}{h_1^2} - 1\right) \tag{A.20}$$

It can be seen that the normal stress $\sigma_x^{(1)}(x = L, z)$ is not zero everywhere on the crack surface $x = L$ (only its average $\tilde{\sigma}_x^{(1)}(x = L)$ is zero); this is a necessary limitation of the "shear-lag" type analysis. Due to the displacement distri-

bution Eq. (A.6) and the assumption of very slow variation of the displacement in the z-direction, the shear stress $\tau_{xz}^{(1)}$ has a linear variation across the thickness of the 90°-layer; this leads to:

$$\tau_{xz}^{(1)}(x,z) = \frac{\tau^*(x)}{h_1} z \tag{A.21}$$

where $\tau^*(x)$ is the interface shear stress. Eqs. (A.20) and (A.21) can be used to express the equivalent stress as a function of x and z,

$$\sigma_{\text{eq}}(x,z) = \left[\sigma_x^{(1)2} + k_{\text{eq}}\tau_{xz}^{(1)2}\right]^{1/2} \tag{A.22}$$

A.2. Numerical assessment of approximation (7)

Approximation (7) is defined by

$$\left\langle \sigma_x^{(1)} g_2(\sigma_{\text{eq}}) \right\rangle_{2h_1} \approx \tilde{\sigma}_x^{(1)} g_2\left(\tilde{\sigma}_x^{(1)}\right) \tag{7}$$

where $g_2(\sigma) = 1 + a_g \sigma^{b_g}$ and the bracket symbol $\langle\,\rangle_{2h_1}$ denotes the average of a function over the thickness of the central layer. Substituting the expressions of the equivalent stress σ_{eq} (Eq. (A.22)) and of the "local stress" $\sigma_x^{(1)}$ (Eq. (A.20)) into the term in the bracket, then averaging over the thickness $2h_1$ of the 90°-layer results in:

$$\left\langle \sigma_x^{(1)} g_2(\sigma_{\text{eq}}) \right\rangle_{2h_1} = F_1\left(\tilde{\sigma}_x^{(1)}, \tau^*, \bar{\sigma}, k_{\text{eq}}, a_g, b_g\right) \tag{A.23}$$

where F_1 is a function of the applied stress $\bar{\sigma}$, the shear stress $\tau^*(x)$, the averaged normal stress $\tilde{\sigma}_x^{(1)}(x)$ between two adjacent cracks and the parameters characterizing the nonlinearity of the material (k_{eq}, a_g, b_g). Let us now consider the right-hand side of approximation (7); using the expression of the averaged normal stress $\tilde{\sigma}_x^{(1)}(x)$ given by Eq. (A.14) results in:

$$\tilde{\sigma}_x^{(1)} g_2\left(\tilde{\sigma}_{\text{x}}^{(1)}\right) = F_2\left(\tilde{\sigma}_x^{(1)}, \bar{\sigma}, a_g, b_g\right) \tag{A.24}$$

where F_2 is a function of $\bar{\sigma}$, $\tilde{\sigma}_x^{(1)}(x)$, a_g and b_g. The numerical simulation of the distributions along the half crack spacing (L) of the two functions F_1 and F_2 (namely the left-hand side and the right-hand side of approximation (7), respectively) is presented in Fig. A1. The comparison between these two functions is studied for several damage states, characterized by crack density $\rho = \frac{1}{2L}$, and at different applied stress levels. For a given crack density, F_1 and F_2 are almost equal when the applied stress is not very high; when the applied stress is greater and close to the value necessary to form a new crack in the 90°-layer, there is some difference between F_1 and F_2. It can be seen in Fig. A2, for a small value ($\rho = 2\ \text{cm}^{-1}$) or a sufficient high value ($\rho = 5\ \text{cm}^{1}$) of the crack density, that the difference between the two functions over the interval between two adjacent cracks is acceptable up to a very high applied stress level (600 MPa for $\rho = 2\ \text{cm}^{-1}$ or 700 MPa for $\rho = 5\ \text{cm}^{1}$), except near the crack surface ($x = L$). In fact, at the crack position, stresses are zero, so both F_1 and F_2 equal zero. The approximation is therefore also reasonable near the crack position. For a very high crack density (about $10\ \text{cm}^{-1}$), the difference between the two functions becomes more important when the applied stress is close to the value necessary to form a new crack at this damage state.

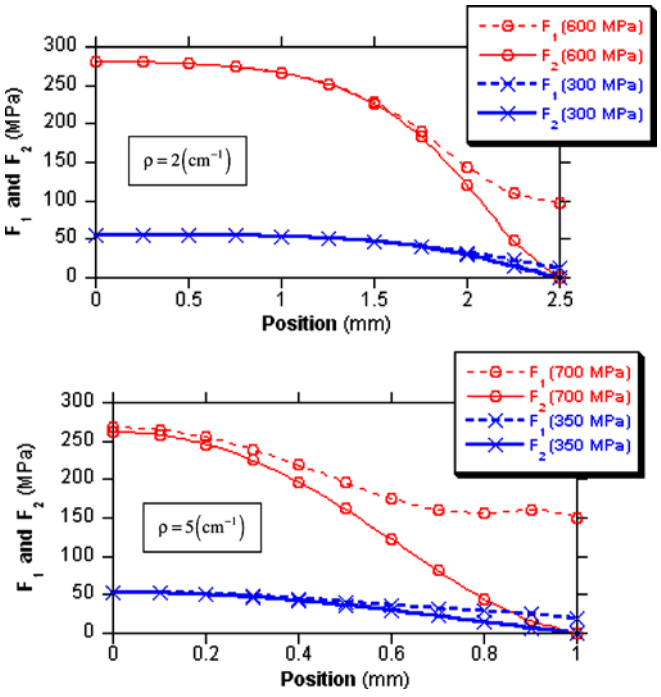

Fig. A1. Comparison between left-hand side (F_1) and right-hand side (F_2) of the approximation (7) for several crack density values at different applied stress levels.

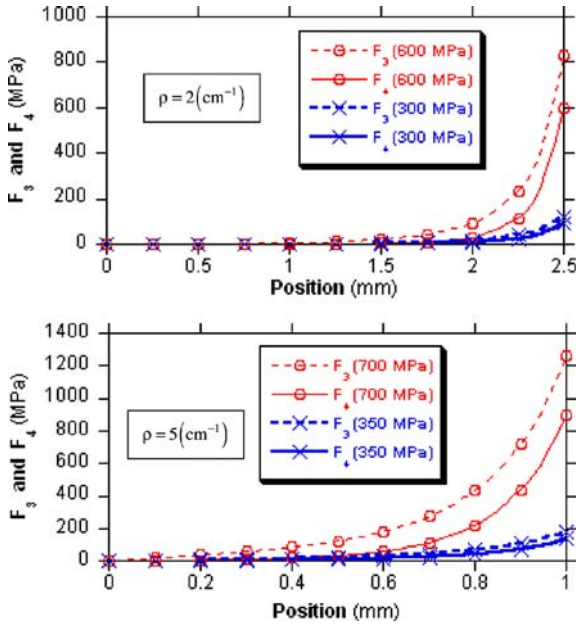

Fig. A2. Comparison between left-hand side (F_3) and right-hand side (F_4) of approximation (10) for several crack density values at different applied stress levels.

A.3. Numerical assessment of approximation (10)

Consider now approximation (10); that is:

$$\tau^* g_2\left(\sigma^*_{eq}\right) \approx \tau^* g_2\left(\tau^* \sqrt{k_{eq}}\right) \tag{10}$$

where $\sigma^*_{eq} = \sigma_{eq}(x, z = h_1)$ is the equivalent stress at the interface $z = h_1$; Substituting the normal stress $\sigma_x^{(1)}(x, z = h_1)$ given by Eq. (A.20) and the interfacial shear stress $\tau^*(x)$ given by Eq. (A.11) into Eq. (A.22), results in the left-hand side and the right-hand side of (10), respectively, in the form:

$$\tau^* g_2\left(\sigma^*_{eq}\right) = F_3\left(\tilde{\sigma}_x^{(1)}, \tau^*, \bar{\sigma}, k_{eq}, a_g, b_g\right) \tag{A.25}$$

$$\tau^* g_2\left(\tau^* \sqrt{k_{eq}}\right) = F_4\left(\tilde{\sigma}_x^{(1)}, \tau^*, \bar{\sigma}, k_{eq}, a_g, b_g\right) \tag{A.26}$$

A numerical comparison between the two functions F_3 and F_4 is presented in Fig. A2 for a small value ($\rho = 2\ \mathrm{cm}^{-1}$) and a sufficient high value ($\rho = 5\ \mathrm{cm}^{-1}$) of the crack density. F_3 and F_4 are nearly equal when the applied stress is not very high. When the applied stress attains the value necessary to form a new crack, there is some difference between the two functions along the interval ($-L < x < +L$), except near its center ($x = 0$). The difference is more important near the crack positions and it is due to the locally non-zero normal stress on the crack surfaces at $z = h_1$ predicted by the "shear-lag" analysis. However, it must be remembered that a fully 3D analysis would predict a zero shear stress both at the center of the interval between adjacent cracks ($x = 0$) and at crack positions ($x = L$).

A.4. Conclusions

The accuracy of both approximations depends upon the applied stress level, the damage state of the laminate as well as the nonlinear character of the considered material. If the applied stress is small or the crack density is low, the approximations are appropriate. They may become very inaccurate when the stress grows at a high damage level. In the special case when the layers are assumed to display a linear elastic behaviour, the above-mentioned numerical simulations show that these approximations are acceptable up to some high applied stress level at a high damage state (namely L small). These results suggest that both approximations are admissible in the studied conditions.

References

[1] Ogi K, Takao Y. Modeling of time-dependent behaviour of deformation and transverse cracking in cross-ply laminates. Adv Compos Mater 2001;10(1):39–62.

[2] Raghavan J, Meshii M. Time-dependent damage in carbon fibre-reinforced polymer composites. Composites Part A: Appl Sci Manufact 1996;27:1223–7.

[3] Moore RH, Dillard DA. Time-dependent matrix cracking in cross-ply laminates. Compos Sci Technol 1990;39:1–12.

[4] Lafarie-Frenot MC. Influence of strain rate and temperature on transverse ply cracking of CFRP laminates. In: The 10th European conference on composite materials (ECCM 10), Bruges, Belgique; 2002.

[5] Akshantala NV, Brinson LC. A damage evolution model for viscoelastic composite laminates. J Compos Technol Res 2001;23(1):3–14.

[6] Nguyen TH, Lafarie-Frenot MC, Gamby D. Influence of loading rate on transverse ply crack growth in aeronautical CFRP laminates. In: The 11th European conference on composite materials (ECCM 11), Rhodes, Greece; 2004.

[7] Lafarie-Frenot MC, Gamby D, Nguyen TH. Experimental and numerical analysis of loading rate and temperature effects on matrix cracking in CFRP laminates. Proc Inst Mech Eng Part L: J Mater Des Appl 2004;218:47–53.

[8] Zhang Y, Xia Z, Ellyin F. Nonlinear viscoelastic micromechanical analysis of fibre-reinforced polymer laminates with damage evolution. Int J Solids Struct 2005;42:591–604.

[9] Kennedy TC, Wang M. Three-dimensional, nonlinear viscoelastic analysis of laminated composites. J Compos Mater 1994;28(10):902–25.

[10] Schapery R. Nonlinear viscoelastic and viscoplastic constitutive equations based on thermodynamics. Mech Time-Depend Mater 1997;1(2):209–40.

[11] Gamby D, Blugeon L. On the characterization by Schapery's model of non-linear viscoelastic materials. Polym Test 1987;7: 137–147.

[12] Allix O, Ladeveze P, Le Dantec E, Vittecoq E. Damage mechanics for composite laminates under complex loading. In: Boehler JP, editor. Yielding, damage and failure of anisotropic solids, EGF5. London: Mechanical Engineering Publications; 1990. p. 551–69.

[13] Schapery RA. Correspondence principle and a generalized *J* integral for large deformation and fracture analysis of viscoelastic media. Int J Fract 1984(25):195–223.

[14] Press WH, Teukolsky SA, Vetterling WT, Flannery BP. Numerical recipes in Fortran. Cambridge: Cambridge University Press; 1992.

[15] Nguyen TH. Etude expérimentale et modélisation de la cinétique d'endommagement par multifissuration matricielle dans des stratifiés carbone/époxyde soumis à des chargements monotones à vitesse imposée ou à des chargements de fatigue à fréquence imposée ("Experimental study and modelling of damage kinetics induced by matrix transverse cracking in carbon/epoxy laminates subjected to monotonic loading or fatigue loading). PhD thesis, Université de Poitiers, Poitiers, France; 2005.

[16] Vinogradov V, Hashin Z. Probabilistic energy based model for prediction of transverse cracking in cross-ply laminates. Int J Solids Struct 2005;42:365–92.

[17] Han YM, Hahn HT, Croman RB. A simplified analysis of transverse ply cracking in cross-ply laminates. Compos Sci Technol 1988;31:165–77.

[18] Ogin SL, Smith PA, Beaumont PWR. Transverse ply crack growth and associated stiffness reduction during the fatigue of a simple crossply laminate. CUED/C/MATS/TR.105, Engineering Department, Cambridge University, UK; 1984.

[19] Henaff-Gardin C, Lafarie-Frenot MC, Gamby D. Doubly periodic matrix cracking in composite laminates. Part 1: General in-plane loading. Compos Struct 1996;36:113–30.

[20] Landis CM, Pardoen T, Hutchinson JW. Crack velocity dependent toughness in rate dependent materials. Mech Mater 2000;32: 663–678.

[21] Rottler J, Barsky S, Robbins MO. Cracks and crazes: on calculating the macroscopic fracture energy of glassy polymers from molecular simulations. Phys Rev Lett 2002;89(14):148304.

[22] Liang J, Zhang Z, Prévost JH, Suo Z. Time-dependent crack behavior in an integrated structure. Int J Fract 2004;125:335–48.

[23] Liang J, Huang R, Prévost JH, Suo Z. Thin film cracking modulated by underlayer creep. Exp Mech 2003;43(3):269–79.

[24] Lafarie-Frenot MC, Hénaff-Gardin C. Formation and growth of 90° ply fatigue cracks in carbon/epoxy laminates. Compos Sci Technol 1991;40(3):307–24.

[25] Parry DJ, Al-Hazmi FS. Stress–strain behaviour of IM7/977-2 and IM7/APC2 carbon fibre composites at low and high strain rates. J Physique IV France 2003;110:57–62.

[26] Gamby D, Lafarie-Frenot MC, Vinet A, Guedra-Degeorge D. The prediction of the long-term mechanical behaviour of aeronautical laminates. Compos Sci Technol 2001;61:439–43.

[27] Schapery RA. Further development of a thermodynamic constitutive theory: stress formulation, Purdue Research Foundation, Research project number 4958; 1969.